**Geomechanics and Engineering**, *Vol. 20, No. 2 (2020) 103-112*
DOI: https://doi.org/10.12989/gae.2020.20.2.103


# Dynamic response characteristics of crossing tunnels under heavy-haul train loads

Jie Dong[1], Shuai Zhong[1], Hai-long Wang*[1] and Zhi-hui Wu[2]

[1]*College of Civil Engineering, Hebei University of Architecture, Zhangjiakou 075000, Hebei, People's Republic of China*
[2]*School of Civil Engineering, Chongqing University, Chongqing 400045, People's Republic of China*

*(Received August 29, 2019, Revised January 1, 2020, Accepted January 2, 2020)*

**Abstract.** The dynamic response of crossing tunnels under heavy-haul train loads is still not fully understood. In this study, based on the case of a high-speed tunnel underneath an existing heavy-haul railway tunnel, a model experiment was performed to research the dynamic response characteristics of crossing tunnels. It is found that the under-crossing changes the dynamic response of the existing tunnel and surrounding rock. The acceleration response of the existing tunnel enhances, and the dynamic stress of rock mass between crossing tunnels decreases after the excavation. Both tunneling and the excitation of heavy-haul train loads stretch the tunnel base, and the maximum tensile strain is 18.35 με in this model test. Then, the measured results were validated by numerical simulation. Also, a parametric study was performed to discuss the influence of the relative position between crossing tunnels and the advanced support on the dynamic behavior of the existing tunnel, where an amplifying coefficient of tunnel vibration was introduced to describe the change in acceleration due to tunneling. These results reveal the dynamic amplifying phenomenon of the existing tunnel during the new tunnel construction, which can be referred in the dynamic design of crossing tunnels.

**Keywords:** crossing tunnels; heavy-haul train loads; dynamic response; model experiment; numerical simulation

## 1. Introduction

Railways are essential infrastructures that provide material and passenger transportation. With the implementation of national strategies such as the coordinated development of Beijing-Tianjin-Hebei, the density of the transportation network in North China has increased year by year. Consequently, the case of new tunnels excavating beneath existing heavy-haul railway tunnels starts to appear. Tunneling inevitably harms the existing tunnel (Choi and Lee 2010, Avgerinos *et al.* 2017). At the same time, it is necessary to discuss further the safety of crossing tunnels under the excitation of heavy-duty trains.

There are many methods used to research the influence of adjacent tunneling on existing tunnels, such as analytical approaches, numerical simulations, field tests, and physical model experiments. Multiple analytical solutions have been proposed for analyzing the mechanical behavior of the existing tunnel or pipeline (Klar *et al.* 2005, Vorster *et al.* 2005, Zhang and Huang 2014). As the rapid development of computer techniques, it is possible to reproduce the three-dimensional interaction between new tunnels and existing tunnels. Avgerinos *et al.* (2017) carried out a series of numerical analyses to reveal the internal force and deformation of the existing tunnel during tunneling. A parametric study was also conducted to analyze the effect of the face pressure of EPBM. Nawel and Salah (2014) study the interaction response of parallel tunnels by using Plaxis, and the influence of tunnel depth, size and position was analyzed. Liu *et al.* (2009) investigated the mechanical response of the shotcrete lining and rock bolts during the excavation of the new tunnel by using a full three-dimensional finite element analysis. Besides, field tests and physical model experiments are widely used because they can genuinely reflect the interaction between crossing tunnels. To research the influence of the earth pressure coefficient, the clearance distance, and the size of the existing tunnel on the interaction between crossing tunnels, Choi and Lee (2010) performed a series of experimental model tests, this study shows how changes in the stress state and the parameter of the existing tunnel influence the mechanical behaviors of the new tunnel. Ng *et al.* (2013, 2016) proposed a tunneling simulation technique to simulate the volume and weight losses, and they conducted a series of three-dimensional simulation to study the effect of tunnel shapes on the tunnel interaction and the mechanical response of the new tunnel. Based on 18 cases of shield tunneling beneath existing tunnels, Jin *et al.* (2018) found that the existing tunnel lining emerges bending deformation during the new tunnel advancement, which leads to the continuous increase of the stress of the tunnel lining.

When existing heavy-haul railway tunnels are in operation during the excavation of new tunnels, it is necessary to draw attention to the impact of the heavy-haul train load on the structure of crossing tunnels. The dynamic response of the tunnel and the surrounding soil or rock under train load was intensively studied during the last few

*Corresponding author, Ph.D., Professor
E-mail: wanghailong1965@hotmail.com


http://www.techno-press.org/?journal=gae&subpage=7
ISSN: 2005-307X (Print), 2092-6219 (Online)

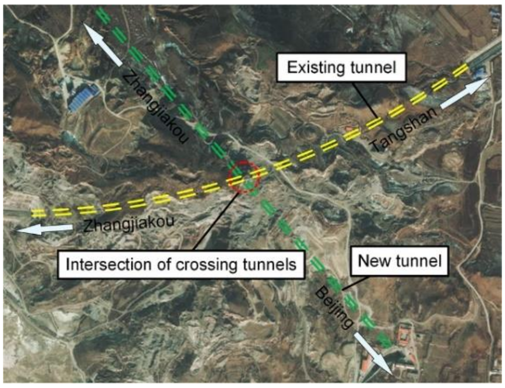


(a) Location

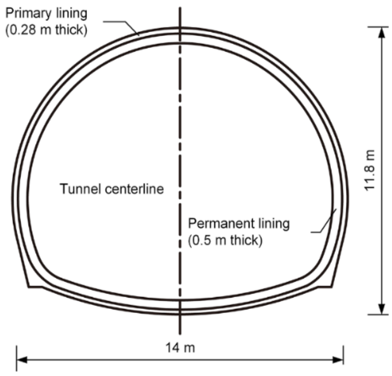


(b) Tunnel section

Fig. 1 Location and typical section of crossing tunnels

decades. Based on the three-dimensional FE analysis, the influence of the water content of soil on the dynamic behavior of the pedestrian tunnel under train loads was studied by Farghaly and Kontoni (2018). Some researchers carried out a series of physical model tests and numerical analyses to investigate the dynamic response characteristics of shield tunnels considering the joint in linings (Gharehdash and Barzegar 2015, Yang *et al.* 2018). Liu *et al.* (2016) studied the dynamic response of the tunnel invert under special multi-directional loads. A fatigue damage model, including stress level parameters, was proposed to analyze and quantify the influence of train vibration loads on tunnel structure. Based on a case of a high-speed tunnel crossing underneath a high-speed railway, Yi *et al.* (2019) performed a 1/10 proportional model test and numerical analysis to study the cumulative deformation of the lining under long-term cyclic loading of high-speed trains. A limited number of studies related to the dynamic response of crossing tunnels under train loads have been conducted. Lai *et al.* (2016) presented a case study of the crossing tunnels of the metro tunnel (the lower tunnel) and the road tunnel (the upper tunnel). They investigated the vibration and stress characteristics of the metro tunnel under the motor vehicle load and metro train load by numerical analyses. They also identified the affected area and the dangerous parts of the metro tunnel. Yan *et al.* (2018) conducted the 3D dynamic FE simulation concerning joints between segments to study the dynamic response of the segment lining of crossing tunnels. The train loads were applied in the lower tunnel to reveal the influences of trains on the upper tunnel.

However, little attention has been devoted to the dynamic response of the existing tunnel under heavy-duty train excitation during the excavation of a new tunnel constructing beneath it. Relative to the metro train load or the high-speed train load, the heavy-haul train load has the characteristics of large amplitude, low frequency, and long duration. Thus vibration problems of tunnel structure under heavy-haul train load are more serious. In this study, based on the case of a high-speed tunnel crossing beneath an existing heavy-haul railway tunnel, a physical model experiment was carried out to study the dynamic characteristics of the existing tunnel and the rock mass between crossing tunnels. Moreover, three-dimensional numerical simulation analyses were performed to research the influencing factors of clearance distance, crossing angle, and advanced support on the dynamic characteristics of the existing tunnel.

## 2. Project overview

The Beijing-Zhangjiakou high-speed railway is the key supporting transportation infrastructure of the 2022 Beijing Winter Olympics. This railway will be an important transportation hub connecting the two areas of Beijing and Zhangjiakou. Influenced by factors, such as the horizontal and vertical route selection of the new tunnel, the new high-speed railway tunnel will excavate beneath the existing heavy-haul railway tunnel in the design range section DK173+862-DK174+057 of the new tunnel (Fig. 1(a)). The clearance distance between crossing tunnels is only 16 m, and the skew of crossing angle is 76°. According to a geological survey, the strata at the intersection of the new tunnel and the existing tunnel are moderately weathered tuff and strongly weathered tuff, respectively. Both the new tunnel and the existing tunnel are single bore tunnels with double tracks, and the tunnel section is 11.8 m high and 14.0 m wide (Fig. 1(b)). It should be pointed that heavy haul trains will periodically pass through the existing tunnel during the construction of the new tunnel.

## 3. Model experiment methods

### 3.1 Model container and loading system

The model experiment was implemented in a rigid container. The container size is 1600 mm × 1600 mm × 1600 mm (Fig. 2). The 15-mm-thick transparent toughened glass was installed at the front and back sides of the container to facilitate the observation during testing. A 10-mm-thick polystyrene foam board was placed to the left side, right side, and bottom side to reduce the wave reflection effect at boundary during the dynamic loading process (Pak and Guzina 1995). Additionally, smooth polyethylene films were added to decrease the friction effect between the container and the model material.

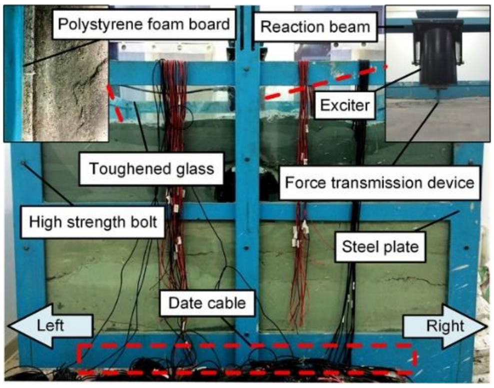


Fig. 2 Front view of the model container

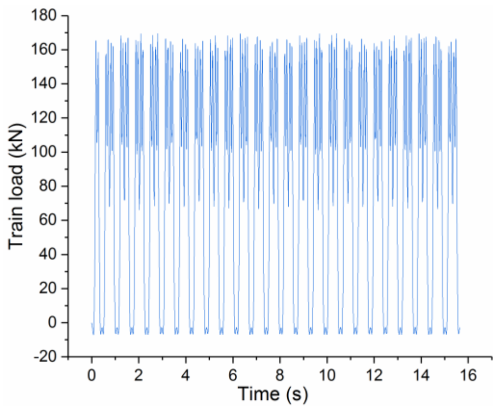


Fig. 3 Time-history of input force (prototype scale)

Loading system, which comprises the reaction beam, the excitation equipment, and the force transmission device, was located on the upper part of the model container. The reaction beam was located at the longitudinal centerline of the container, and it was made of high-strength alloy steel with high shock resistance and toughness. A JC-50 multifunctional exciter was installed in the center of the reaction beam to transmit the exciting force to the tunnel invert. Based on the train-track-subgrade system model, the vibration force on the ballast layer induced by C80 heavy-haul train with a speed of 70 km/h was selected as the excitation vibration source (Fig. 3).

### *3.2 Similarity relationship*

In this 1g model experiment for the dynamic response of crossing tunnels, the key physical quantities were length $l$, acceleration $a$, density $\rho$, Young's modulus $E$, stress $\sigma$, strain $\varepsilon$, Poisson's ratio $\mu$, cohesion $c$, friction angle $\varphi$, force $F$, time $T$ and so on (Jeon *et al.* 2004). Thereby the solution equation for these physical parameters can be expressed as

$$f(l,a,\rho,E,\sigma,\varepsilon,\mu,c,\varphi,F,T)=0 \tag{1}$$

Choosing length $l$, acceleration $a$, and density $\rho$ as the fundamental parameter, the other parameters can be deduced by using the Buckingham π Theorem (Carpinteri and Chiaia 1996), we have:

$$f(\pi_1,\pi_2,\pi_3,\pi_4,\pi_5,\pi_6,\pi_7,\pi_8)=0 \tag{2}$$

Fig. 4 Preparation of model materials

Table 1 Physical parameters of prototype materials and model materials

| Name | | $\rho$ (kg/m$^3$) | $E$ (MPa) | $\mu$ | $c$ (kPa) | $\varphi$ (°) |
|---|---|---|---|---|---|---|
| SW tuff | Prototype | 2000-2400 | 900-1700 | 0.40-0.45 | 180-230 | 23-28 |
| | Model | 2190 | 28 | 0.40 | 4.6 | 26 |
| MW tuff | Prototype | 2100-2500 | 2000-3500 | 0.30-0.40 | 200-500 | 30-35 |
| | Model | 2310 | 63 | 0.33 | 7.2 | 34 |
| Lining | Prototype | 2400-2500 | 27000-29000 | 0.20-0.22 | 2000-2200 | 50-55 |
| | Model | 2300 | 570 | 0.20 | 44 | 51 |

*SW tuff: Strongly weathered tuff; MW tuff: Moderately weathered tuff

$$\begin{gathered}\pi_1=E/la\rho,\ \pi_2=\sigma/la\rho,\ \pi_3=\varepsilon,\ \pi_4=\mu,\\ \pi_5=c/la\rho,\ \pi_6=\varphi,\ \pi_7=F/l^3a\rho,\ \pi_8=T/l^{0.5}a^{-0.5}\end{gathered} \tag{3}$$

To ensure the similarity between the model (marked with subscript "$m$") and the prototype (marked with subscript "$p$"), the π relation of the model and prototype should be same, which can be denoted as

$$\begin{cases} f(\pi_1,\pi_2,\pi_3,\pi_4,\pi_5,\pi_6,\pi_7,\pi_8)_p=0\\ f(\pi_1,\pi_2,\pi_3,\pi_4,\pi_5,\pi_6,\pi_7,\pi_8)_m=0\end{cases} \tag{4}$$

$$\begin{cases}\pi_{1m}=\pi_{1p}\\ \pi_{2m}=\pi_{2p}\\ \vdots\\ \pi_{8m}=\pi_{8p}\end{cases} \tag{5}$$

The ratio of similitude ($C$) is the ratio between the prototype physical quantities and the model physical quantities. Considering the experimental condition and objective, the selected similarity ratio of length, acceleration, and density were $C_l$=50, $C_a$=1 and $C_\rho$ =1. Thus, the similarity ratios of the other physical parameters were $C_\varepsilon$=$C_\mu$=$C_\varphi$=1, $C_E$=$C_\sigma$=$C_c$=50, $C_F$=125000 and $C_T$=7.071.

### *3.3 Model materials*

Selecting density, elastic modulus, cohesion, and friction angle as the control parameters of model materials, a series of laboratory orthogonal tests were conducted to determine the model materials of the surrounding rock and lining (Fig.

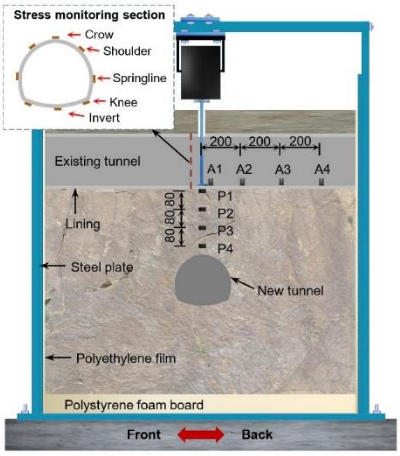

Fig. 5 Layout of sensors (unit: mm)

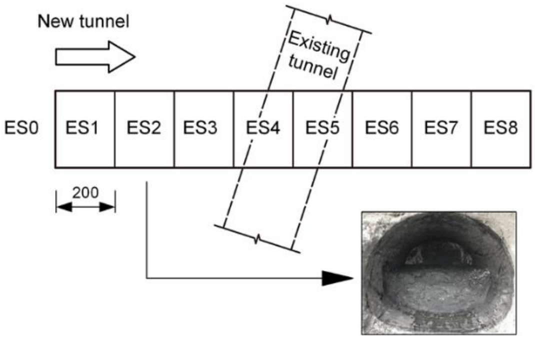

Fig. 6 Excavation steps of the new tunnel (unit: mm)

4). The model materials of the surrounding rock included gypsum, quartz sand, barite, iron powder, glycerin, and water. Among them, the main binder was gypsum. Barite and iron powder was mainly used to adjust the unit weight of the surrounding rock, and the cohesion and the friction angle were regulated on glycerin. Mixtures of high-strength gypsum, cement, and water were employed as the model materials of the lining. The layered pouring method was adopted to ensure the solid continuity of the surrounding rock. The height of each layer is 5 cm. The mechanical parameters of both prototype materials and model materials are shown in Table 1.

### 3.4 Instrumentation

The NI9234 acceleration measurement system and the NI9237 dynamic strain instrument were used to measure the acceleration, the dynamic vertical stress, and the dynamic strain in this test. Fig. 5 presents the layout of accelerometers, dynamic soil pressure gauges, and strain gauges. The accelerometers, which were respectively A1, A2, A3, and A4, were arranged outward from the intersection along the existing tunnel centerline with a spacing of 200 mm to measure the vibration of the lining. The dynamic soil pressure gauges, which were respectively P1, P2, P3, and P4, were arranged directly below the vibration source with a spacing of 80 mm to study the attenuation law of dynamic stress in the interlayer of the surrounding rock. The lining at the intersection is often in the unfavorable state. Thus, the strain monitoring section was located near the intersection. Eight strain gauges were installed on the outer of the lining to measure the hoop strain of the existing tunnel.

### 3.5 Experimental process

After the fabricating and curing of the model, the bench excavation method was used to simulate the practical excavation. According to the design excavation scheme of the new tunnel and similarity ratio, the upper bench is 120 mm high, the lower bench is 82 mm high, and the bottom excavation is 38 mm high. This paper focused on the dynamic characteristics of crossing tunnels under nine typical excavation steps (ES), and every ES included upper bench excavation, lower bench excavation, and bottom excavation (Fig. 6). The train load was applied when each ES completed and the transducer readings stabilized. Also, the next excavation was carried out after the completion of data acquisition.

## 4. Results analysis of the model experiment

According to the similarity ratio, the measured results were converted into the prototype scale to facilitate subsequent analyses.

### 4.1 Acceleration of the existing tunnel

The typical acceleration time-history curves of the lining response under train loads are shown in Fig. 7. The vibration acceleration curve has distinct vibration peaks, and the loading cycle of the wheel pair can be observed. The peak particle acceleration (PPA) was used to describe the vibration response of the tunnel lining. The PPA represents the maximum absolute value of the particle acceleration.

Fig. 8 shows the PPA at A1, A2, A3, and A4 changed along with ES. As the new tunnel excavation, the PPA of the existing tunnel lining increased. The excavation process was divided into stage I (ES0-ES2), stage II (ES3-ES5), and stage III (ES6-ES8) according to the PPA variation characteristic. In stage I, the excavation of the new tunnel had little disturbance to the existing tunnel. Thus, the acceleration response characteristics of the existing tunnel lining are hardly affected. In stage II, the initial stress state of the surrounding rock beneath the existing tunnel had been changed, and the rock mass between crossing tunnels began to open and crack. Therefore, the overall rigidity of the rock pillar decreased, which resulted in the dramatic increase of PPA. In stage III, the new tunnel had passed the existing tunnel by a certain distance. The increasing trend of PPA slowed down owing to the rock pillar little disturbed by tunneling far away. However, with the increase of the distance from the vibration source, the trend of the PPA increasing with the advancement of the new tunnel gradually weakened. During the entire excavation process, the PPA at A1, A2, A3, and A4 increased by 18.1%, 11.3%, 3.3%, and 1.2%, respectively. There are two reasons for this phenomenon. On the one hand, due to material damping and geometrical diffusion, the acceleration response

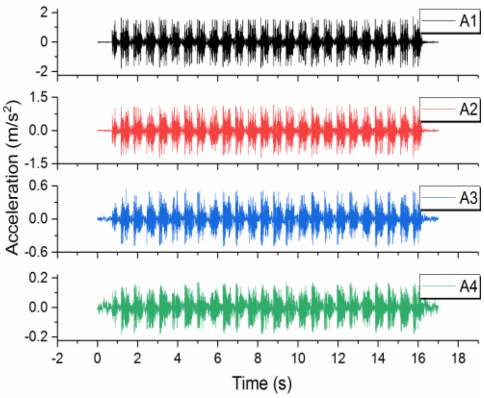


(a) Before the excavation of the new tunnel

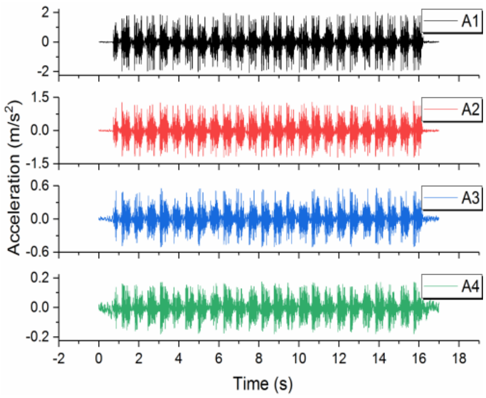


(b) After the excavation of the new tunnel

Fig. 7 Time-history curves of acceleration

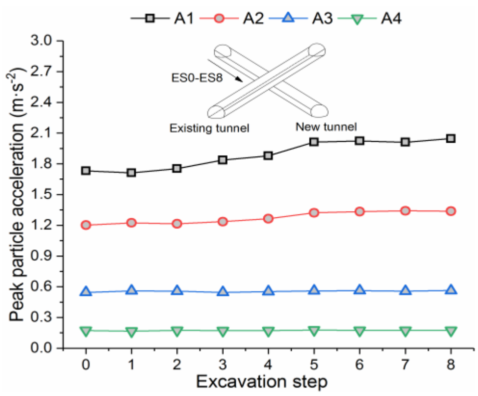


Fig. 8 Variation of peak particle acceleration with ES

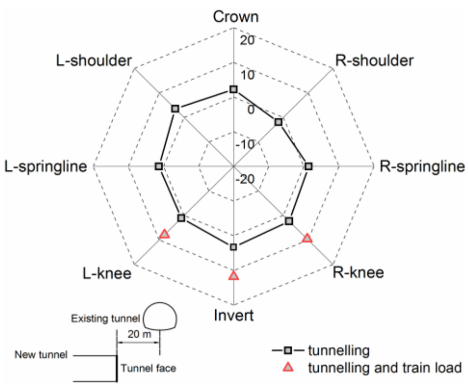


(a) Before the under-crossing

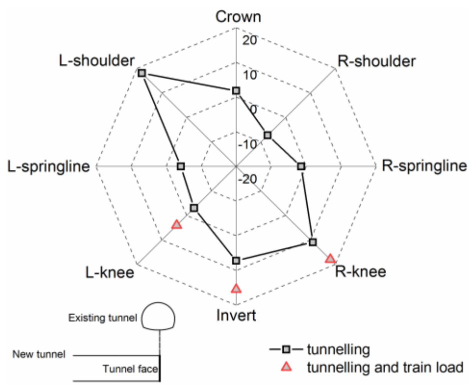


(b) During the under-crossing

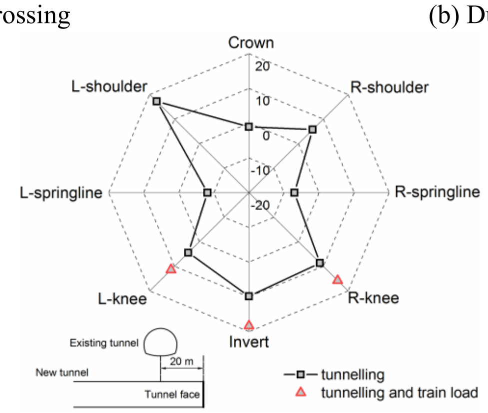


(c) After the under-crossing

Fig. 9 Induced hoop strain in typical excavation stages

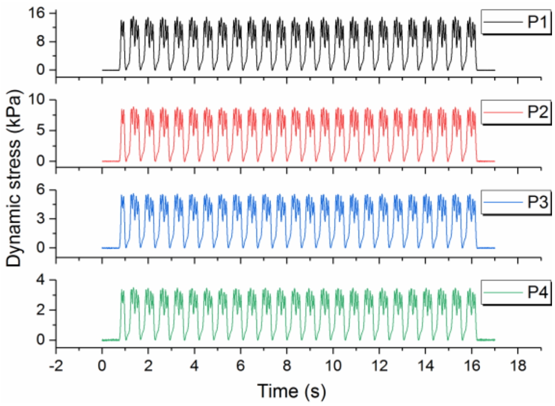


(a) Before the excavation of the new tunnel

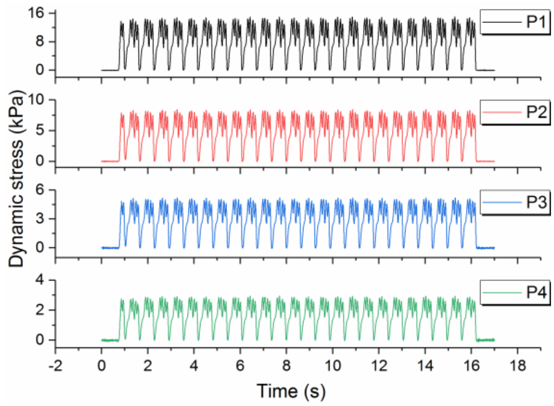


(b) After the excavation of the new tunnel

Fig. 10 Time-history curves of dynamic vertical stress

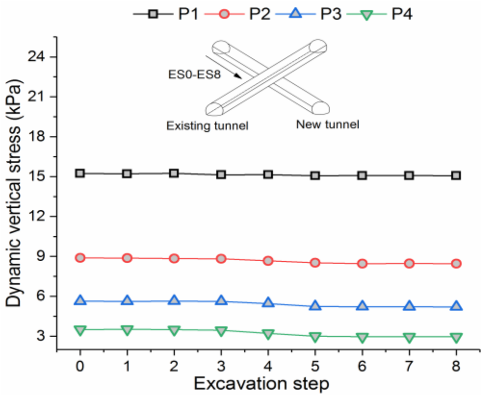


Fig. 11 Variation of dynamic vertical stress with ES

decreases with increasing the distance from the vibration source. On the other hand, it may be that the acceleration response characteristics of the existing tunnel are only affected within a specified range from the intersection.

It should be noted that the presence of the lower tunnel resulted in a significant amplification of the PPA of the existing tunnel lining. Given that the existing tunnel was subjected to long-term cyclic loading of heavy-haul trains, the amplification of dynamic response hurts the safety of the tunnel structure, which will cause the intersection area of the existing tunnel to be more susceptible to damage than other areas.

### *4.2 Induced hoop strain of the existing tunnel*

The excavation of the new tunnel leads to the redistribution of the stress state of the surrounding rock, which causes induced strain in the existing tunnel. Also, the stress state of lining will be extremely complicated under the excitation of heavy-haul trains. In this part, the influence of tunneling and heavy-duty train excitation on the tunnel structure was analyzed by induced hoop strain on the outer surface of the lining. The distributions of induced hoop strain in three typical excavation stages are shown in Fig. 9, where the tensile strain is positive, and the compressive strain is negative.

The effect of tunneling on the existing tunnel was first analyzed. When the tunnel face was 20 m from the intersection, the surrounding rock beneath the intersection was less disturbed. Therefore, the induced hoop strain in the outer face of the lining was small, and the maximum value was only 3.51 με. When the tunnel was excavated to the intersection, the tensile strain was generated at the crown, invert, r-knee and l-shoulder, and the induced strain in rest parts was the compressive strain. Furthermore, the induced strain of the existing tunnel exhibited obvious asymmetry. This phenomenon is mainly because the tunneling released the surrounding rock pressure at the left bottom of the monitoring section, resulting in non-uniform deformation of the tunnel. When the tunnel face was 20 m away from the intersection, the surrounding rock pressure at both left and right bottom of the monitoring section were released. Therefore, the induced hoop strain was approximately symmetrically distributed. In addition to the monitoring point at the springline, the induced hoop strain in the other positions was the tensile strain.

The excitation load of the heavy-haul train mainly affects tunnel base structures (Yang *et al.* 2018, Zhang *et al.* 2018). Hence, only the hoop strain induced by the excitation load in the invert and knee was analyzed. The tensile strain was generated on the outer of the tunnel base under heavy-haul train loads, and the value of hoop strain induced by train loads in different excavation stages was similar. Both the under-crossing and the excitation of the heavy-haul train caused the tunnel base to stretch circumferentially, and the maximum value of tensile strain was 18.35 με in the test. If the hoop tensile strain was close to 150 με before the excavation, the lining might crack during the new tunnel construction (*Ng et al.* 2013). Moreover, the tunnel base state of the existing tunnel is usually poor due to factors such as the groundwater scour and the long-term dynamic load of trains, so the tunnel base is more prone to damage during the construction of the new tunnel. Therefore, the monitoring of the tunnel base should be strengthened.

### *4.3 Dynamic stress of the surrounding rock between crossing tunnels*

Fig. 10 shows the typical dynamic stress time-history curves of P1, P2, P3, and P4 under train loads. The vertical dynamic stress gradually decreased with the increase of the distance from the vibration source. For example, before the excavation of the new tunnel, the dynamic stress at P2, P3, and P4 attenuated by 41.6%, 63.0%, and 76.9% than that at P1. The decay rate was the fastest from P1 to P2, and then the decay rate was slowed down.

Fig. 11 indicates that the variation of dynamic stress at P1, P2, P3, and P4 with ES. With the advancement of the new tunnel, the attenuation law of dynamic stress in the surrounding rock changed, and the dynamic stress at P1, P2, P3, and P4 decreased. Specifically, the dynamic stress at P4 was 3.52 kPa in ES0, and it decreased rapidly from ES3 to ES5. The final value of dynamic stress at P4 was 2.96 kPa, which was 15.9% lower than the initial value. Moreover, the attenuation amplitudes of P1, P2, and P3 were 1.1%, 4.7%, and 7.5%, respectively. It can be seen that the dynamic stress attenuation of the monitoring point near the new tunnel was large. Here, the “floating surface” below the monitoring point gradually increased with the advancement of the lower tunnel, and the surrounding rock deformed toward the new tunnel under the dynamic load so that the stress was released to a certain extent. The closer the monitoring point is to the lower tunnel, the higher the degree of stress releases, which makes the dynamic stress drop larger.

Table 2 Simulation programs

| Case | Clearance distance (m) | Crossing angle (°) | Support measure for the new tunnel |
|---|---|---|---|
| 1 | 16 | 76 | None |
| 2 | 7, 14, 21, 28 | 90 | Primary lining |
| 3 | 7 | 90, 75, 60 | Primary lining |
| 4 | 7 | 90 | Primary lining, Advanced support + primary lining |

Table 3 Physical parameters of the numerical model

| Name | $\rho$ (kg/m$^3$) | $E$ (MPa) | $\mu$ | $c$ (kPa) | $\varphi$ (°) |
|---|---|---|---|---|---|
| Strongly weathered tuff | 2190 | 1400 | 0.40 | 230 | 26 |
| Moderately weathered tuff | 2310 | 3150 | 0.33 | 360 | 34 |
| Grounting reinforcement area | 2250 | 2500 | 0.35 | 470 | 30 |
| Lining | 2300 | 28500 | 0.20 | | |
| Packed layer | 2300 | 28000 | 0.20 | | |
| Ballast layer | 2200 | 21500 | 0.27 | | |
| Pipe roof | 3300 | 93000 | 0.2 | | |

## 5. Three-dimensional numerical analysis

### 5.1 Numerical model description

To verify the measured result and further research the influencing factors of clearance distance, crossing angle, and the advanced supports on the dynamic characteristics of crossing tunnels, numerical back-analysis of the model experimental and the other seven extending conditions were conducted by using the finite-difference program FLAC3D (Table 2).

The simulation parameters for numerical back-analysis were obtained by scaling those of the model test, and the loading method was the same as that in the model test.

In the extending conditions, the surrounding rock was considered as strongly weathered tuff to exclude the influence of rock classes on the dynamic characteristic. The existing tunnel structure consisted of the permanent lining, the packed layer, and the ballast layer, wherein the lining had a thickness of 0.5 m, the packed layer had a thickness of 1.2 m, and the thickness of the ballast layer was 0.24 m. The new tunnel structure ignored the permanent lining, and the primary lining thickness is 0.28 m. The pipe roofs (30 m long and 108 mm in diameter) were installed with a spacing of 0.4 m at the tunnel vault. Besides, the multi-point train loads were applied along the existing tunnel centerline to compensate for the shortcomings of the single-point loading in the model test that was difficult to reflect the dynamic affected range of the existing tunnel. To further eliminate the boundary effects, the length of the existing tunnel was enlarged to 200 m.

The surrounding rock was modeled as an elasto-plastic material with Mohr-Coulomb failure criterion, while the lining, the packed layer, and the ballast layer were assumed to behave as a linearly elastic material. The pipe roofs were simulated using the beam structure unit, and the grouting protection effect was reflected by enhancing the strength of the rock mass around pipe roofs. The mechanical parameters of the materials are shown in Table 3.

The element size in this numerical model was smaller than one-eighth of the wavelength of the highest frequency component of the input vibration wave to ensure the numerical accuracy of wave transmission (Gharehdash and Barzegar 2015), and the model mesh was shown in Fig. 12. The fixed boundaries were used in static analyses, and the normal displacement at the four sides and bottom of the model was contained. In the dynamic analyses, the energy loss characteristic of dynamic loads in medium propagation was simulated by Rayleigh damping. According to the FLAC3D manual, the critical damping ratio of 0.5% was selected, and the center frequency was taken as the natural frequency of the model. The quiet boundary was applied during the dynamic analyses to avoid unwanted wave reflections at the boundary.

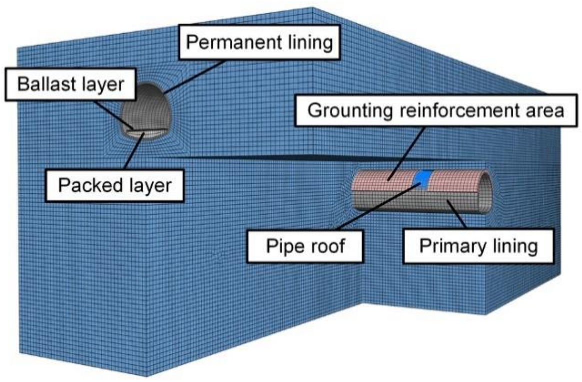


Fig. 12 Numerical model of crossing tunnels

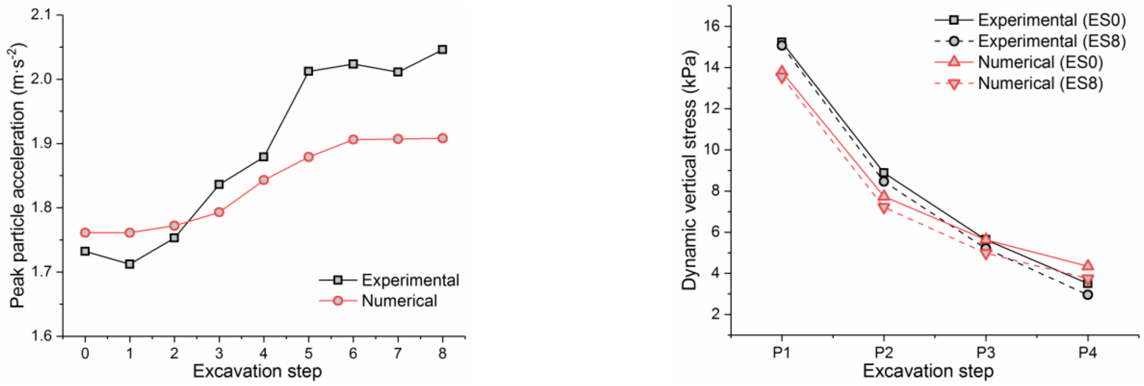


(a) Peak particle acceleration (b) Dynamic vertical stress

Fig. 13 Comparison of the experimental and numerical result

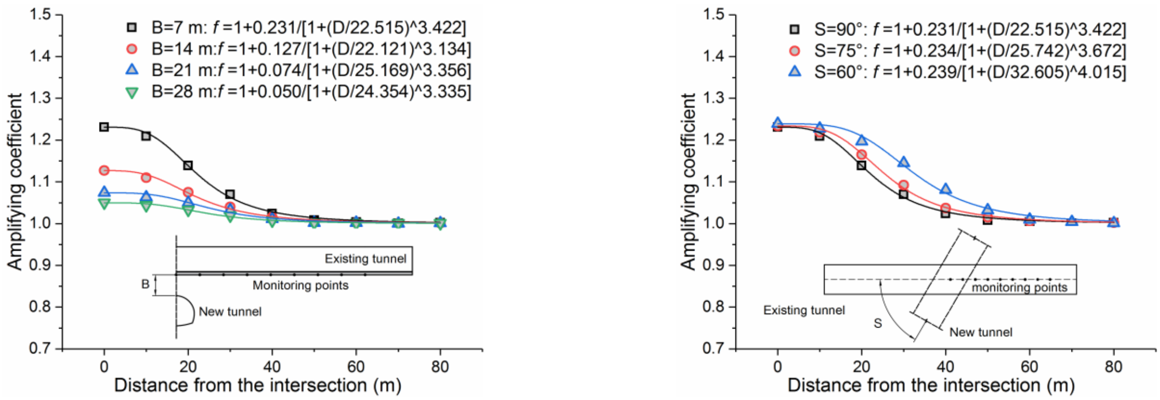


(a) Clearance distance (b) Crossing angle

Fig. 14 Distribution of PPA for different conditions

### *5.2 Comparison of the model experiment and numerical analysis results*

Fig. 13 compares the results of the simulation and the experiment. Fig. 13(a) indicates the PPA of the existing tunnel structure gradually increased with the advancement of the new tunnel both in numerical analyses and model tests. Fig. 13(b) shows the dynamic stress decreased after the excavation, and the pad value increased with the decrease of the distance between the monitoring point and the new tunnel. The computed dynamic stress was comparable to measured dynamic stress. The numerical results and the experimental results are in good agreement, which not only enhances the reliability of the conclusions obtained from the experiment but also suggests that the variation of PPA can be investigated by using numerical analysis.

### *5.3 Influence of the relative position between crossing tunnels on PPA*

In this study, an amplifying coefficient of tunnel vibration was introduced to describe the effect of the new tunnel construction below on the acceleration response of the existing tunnel, which is given by

$$f = \mathrm{PPA}_a / \mathrm{PPA}_b \tag{6}$$

where $f$ is amplifying coefficient of tunnel vibration, $\mathrm{PPA}_a$ and $\mathrm{PPA}_b$ are the PPA at the existing tunnel after and before the new tunnel excavation.

Fig. 14 illustrates the relationship between the amplifying coefficient of tunnel vibration and the horizontal distance between the intersection and the monitoring point ($D$). It is observed that the value of $f$ at the intersection of the existing tunnels was the largest. As the increase of $D$, $f$ gradually decreased because the tunneling had a weaker influence on the far field of the existing tunnel. Therefore, it can be concluded that the amplifying effect of tunnel vibration caused by the under-crossing only appears in the intersection within a particular distance. The $f$-$D$ curve appears "S" shape, and a Logistic function was used to express the relationship between $f$ and $D$.

$$f = 1 + \frac{(f_{\max} - 1)}{(1 + (D/D_0)^P)} \tag{7}$$

where $f_{\max}$ is the maximum value of amplifying coefficient, $D$ is the horizontal distance between the intersection and the monitoring point, $D_0$ and $P$ are the fitting parameters in the Logistic function. The fitting formulas with 95% confidence are given in Fig. 14.

Fig. 14(a) indicates that the amplifying coefficient is closely related to the clearance distance of crossing tunnels. When the clearance distance increased, the excavation of the new tunnel had less effect on the overall stiffness of the

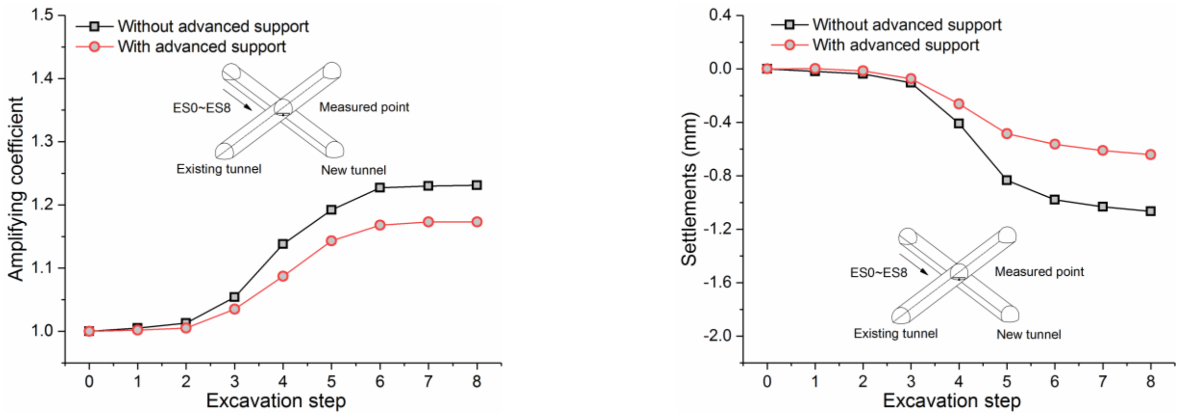


(a) PPA of the existing tunnel (b) Settlement of the existing tunnel

Fig. 15 Influence of advanced support

surrounding rock in between, and the amplification effect of the PPA was significantly weakened. For example, when the clearance was 7 m, $f_{max}$ was 1.231, and it decreased by 8.4%, 12.8%, and 14.7% as the clearance increased to 14 m, 21 m, and 28 m.

Fig. 14(b) shows the distribution of $f$ with crossing angle. With the crossing angle decreased, there was a slight increase in $f$. Among them, when the crossing angle reduces from 90° to 75° and 60°, $f_{\max}$ increased from 1.231 to 1.234 and 1.239. Besides, the decrease of crossing angle enlarged the amplification range of the existing tunnel. The main reason is that the area, where surrounding rock in between is disturbed, increases with the crossing angle decreases. This causes an increase in the affected area of the dynamic response of the existing tunnel.

### *5.4 Influence of advanced support*

For high-risk projects such as heavy-haul crossing tunnels, advanced support is an important measure to ensure safety during the construction of the new tunnel. The engineering analogy method was adopted, and the pipe roof was selected as the advanced support means. By comparing the PPA and settlement of the condition with advanced support and the condition without advanced support, the performance of the advanced support in heavy-haul crossing tunnels was evaluated.

Fig. 15(a) compares the maximum amplifying coefficient of PPA. The amplifying coefficient of PPA was 1.173 in the condition with advanced support, which was 0.058 lower than that in the condition without advanced support. Due to the underneath tunneling, the rock mass in front of the tunnel face becomes loose. However, the pipe roofs bear the load in advance, effectively controlling the looseness and deformation of the surrounding rock, and the overall stiffness of surrounding rock in between is reduced relatively less. Hence, the existing tunnel is less affected by the excavation of the new tunnel, which leads to a small increase in PPA after tunneling. The effect of advanced support was also reflected in controlling the settlement of the existing tunnel. Fig. 15(b) compares the settlement of the two conditions. The settlement reduced by 39.8% in the condition with advanced support.

## 6. Conclusions

Based on the experimental and numerical analyses, this study investigated the variation characteristics of the dynamic response of the existing tunnel and surrounding rock under heavy-haul train loads during the period of new tunnel construction. The key results are summarized as follows:

• With the advancement of the new tunnel, the PPA of the existing tunnel lining was gradually increasing, and PPA was changing sharply when the tunnel face below the intersection. Finally, the increasing rates for A1, A2, A3, and A4 were 18.1%, 11.3%, 3.3%, and 1.2%, respectively. Induced hoop strain was emerged in the existing tunnel due to the excavation of the new tunnel, and undergone a process of redistribution. Both tunneling and the excitation of heavy-haul train loads stretched the tunnel base, and the maximum tensile strain of the tunnel base was 18.35 με. Besides, the dynamic vertical stress of the surrounding rock in between decreased after the construction of the new tunnel. The closer the distance between the monitoring point and the new tunnel was, the higher the attenuation rates of dynamic stress were. And the attenuation rates of P1, P2, P3, and P4 were 1.1%, 4.7%, 7.5%, and 15.9%, respectively.

• The simulation results and the experiment results are in good agreement. Then, an amplifying coefficient of tunnel vibration was introduced, and the influence of the relative position of crossing tunnels on the amplifying coefficient was analyzed by using numerical simulation. According to the numerical analyses, the amplifying effect of tunnel vibration caused by the under-crossing only appears in the intersection within a particular distance, and the amplifying coefficient of monitoring points decreased with the increase of the distance from the intersection. When the clearance distance increased from 7 m to 28 m, the maximum amplifying coefficient decreased by 14.7%. The decrease of the crossing angle enlarged the influenced area of the existing tunnel. Meanwhile, the maximum value of amplifying coefficient increased slightly. The advanced support can decrease the looseness and deformation of the surrounding rock so that the settlement and the increasing trend of PPA were controlled.

Due to the periodicity of train loads, this study intercepted the heavy-duty train load for a specific length of time for loading. It is found that the tunneling of the lower tunnel affects the dynamic response characteristic of the upper tunnel. And the vibration response of the intersection is more significant than that of the conventional region, which will make the lining near the intersection more vulnerable. In the following research, the influence of the amplification effect under long-term loads on the damage characteristics of existing tunnel structures should be studied.

## Acknowledgments

The research described in this paper was financially supported by the Natural Science Foundation of China (NO. 51878242), the Natural Science Foundation of Hebei Province of China (NO. E2017404013) and the Fund for fostering talents of Hebei Province of China (NO. A201901067).

## References

Avgerinos, V., Potts, D.M. and Standing, J.R. (2017), "Numerical investigation of the effects of tunnelling on existing tunnels", *Geotechnique*, **67**(9), 808-822. https://doi.org/10.1680/jgeot.SiP17.P.103.

Carpinteri, A. and Chiaia, B. (1996), "Power scaling laws and dimensional transitions in solid mechanics", *Chaos Solitons Fractals*, **7**(9), 1343-1364. https://doi.org/10.1016/0960-0779(96)00016-1.

Choi, J.I. and Lee, S.W. (2010), "Influence of existing tunnel on mechanical behavior of new tunnel", *KSCE J. Civ. Eng*., **14**(5), 773-783. https://doi.org/10.1007/s12205-010-1013-8.

Farghaly, A.A. and Kontoni, D.P.N. (2018), "Train induced dynamic response of a pedestrian tunnel under a four-track surface railway for different soil water contents", *Geomech. Eng*., **16**(4), 341-353. https://doi.org/10.12989/gae.2018.16.4.341.

Gharehdash, S. and Barzegar, M. (2015), "Numerical modeling of the dynamic behaviour of tunnel lining in shield tunneling", *KSCE J. Civ. Eng*., **19**(6), 1626-1636. https://doi.org/10.1007/s12205-015-0406-0.

Jin, D.L., Yuan, D.J., Li, X.G. and Zheng, H.T. (2018), "Analysis of the settlement of an existing tunnel induced by shield tunneling underneath", *Tunn. Undergr. Sp. Technol*., **81**, 209-220. https://doi.org/10.1016/j.tust.2018.06.035.

Jeon, S., Kim, J., Seo, Y. and Hong, C. (2004), "Effect of a fault and weak plane on the stability of a tunnel in rock - a scaled model test and numerical analysis", *Int. J. Rock Mech. Min. Sci*., **41**(3), 486-486. https://doi.org/10.1016/j.ijrmms.2003.12.021.

Klar, A., Vorster, T.E.B., Soga, K. and Mair, R.J. (2005), "Soil-pipe interaction due to tunnelling: comparison between Winkler and elastic continuum solutions", *Geotechnique*, **55**(6), 461-466. https://doi.org/10.1680/geot.2005.55.6.461.

Lai, J.X., Wang, K.Y., Qiu, J.L., Niu, F.Y., Wang, J.B. and Chen, J.X. (2016), "Vibration response characteristics of the cross tunnel structure", *Shock Vib*. https://doi.org/10.1155/2016/9524206.

Liu, H.Y., Small, J.C., Carter, J.P. and Williams, D.J. (2009), "Effects of tunnelling on existing support systems of perpendicularly crossing tunnels", *Comput. Geotech.*, **36**(5), 880-894. https://doi.org/10.1016/j.compgeo.2009.01.013.

Liu, N., Peng, L.M., Shi, C.H. and Lei, M.F. (2016), "Experimental and model study on dynamic behaviour and fatigue damage of tunnel invert", *Constr. Build. Mater*., **126**, 777-784. https://doi.org/10.1016/j.conbuildmat.2016.09.081.

Nawel, B. and Salah, M. (2015), "Numerical modeling of two parallel tunnels interaction using three-dimensional Finite Elements Method", *Geomech. Eng*., **9**(6), 775-791. https://doi.org/10.12989/gae.2015.9.6.775.

Ng, C.W.W., Boonyarak, T. and Masin, D. (2013), "Three-dimensional centrifuge and numerical modeling of the interaction between perpendicularly crossing tunnels", *Can. Geotech. J*., **50**(9), 935-946. https://doi.org/10.1139/cgj-2012-0445.

Ng, C.W.W., Wang, R. and Boonyarak, T. (2016), "A comparative study of the different responses of circular and horseshoe-shaped tunnels to an advancing tunnel underneath", *Geotech. Lett*., **6**(2), 168-175. https://doi.org/10.1680/jgele.16.00001.

Pak, R.Y.S. and Guzina, B.B. (1995), "Dynamic characterization of vertically loaded foundations on granular soils", *J. Geotech. Eng*., **121**(3), 274-286. https://doi.org/10.1061/(asce)0733-9410(1995)121:3(274).

Vorster, T.E.B., Klar, A., Soga, K. and Mair, R.J. (2005), "Estimating the effects of tunneling on existing pipelines", *J. Geotech. Geoenviron. Eng*., **131**(11), 1399-1410. https://doi.org/10.1061/(asce)1090-0241(2005)131:11(1399).

Yan, Q.X., Song, L.Y., Chen, H., Chen, W.Y., Ma, S.Q. and Yang, W.B. (2018), "Dynamic response of segment lining of overlapped shield tunnels under train-induced vibration loads", *Arab. J. Sci. Eng*., **43**(10), 5439-5455. https://doi.org/10.1007/s13369-018-3147-9.

Yang, W.B., Chen, Z.Q., Xu, Z.Y., Yan, Q.X., He, C. and Kai, W. (2018), "Dynamic response of shield tunnels and surrounding soil induced by train vibration", *Rock Soil Mech*., **39**(2), 537-545. https://doi.org/10.16285/j.rsm.2016.0941.

Yang, W.B., Cui, G., Xu, Z.Y., Yan, Q.X., He, C. and Zhang, Y.Y. (2018), "An experimental study of ground-borne vibration from shield tunnels", *Tunn. Undergr. Sp. Technol*., **71**, 244-252. https://doi.org/10.1016/j.tust.2017.08.020.

Yi, H.Y., Qi, T.Y., Qian, W.P., Lei, B., Pu, B.R., Yu, Y.Y., Liu, Y.X. and Li, Z.Y. (2019), "Influence of long-term dynamic load induced by high-speed trains on the accumulative deformation of shallow buried tunnel linings", *Tunn. Undergr. Sp. Technol*., **84**, 166-176. https://doi.org/10.1016/j.tust.2018.11.005.

Zhang, Z.G. and Huang, M.S. (2014), "Geotechnical influence on existing subway tunnels induced by multiline tunneling in Shanghai soft soil", *Comput. Geotech*., **56**, 121-132. https://doi.org/10.1016/j.compgeo.2013.11.008.

Zhang, Z.Q., Zeng, B.W., Da, C.L. and He, W.P. (2018), "Study on structural service performance of heavy-haul railway tunnel with voided base", *Adv. Civ. Eng*. https://doi.org/10.1155/2018/3510979.

*CC*